J Appl Physiol 111: 75–80, 2011.
First published April 28, 2011; doi:10.1152/japplphysiol.00205.2011.

Imaging of the closed-chest mouse pulmonary circulation using synchrotron radiation microangiography

Takashi Sonobe,[1] Daryl O. Schwenke,[2] James T. Pearson,[3] Misa Yoshimoto,[1] Yutaka Fujii,[1] Keiji Umetani,[4] and Mikiyasu Shirai[1]

[1]*Department of Cardiac Physiology, National Cerebral and Cardiovascular Center Research Institute, Osaka, Japan;* [2]*Department of Physiology, University of Otago, Dunedin, New Zealand;* [3]*Department of Physiology, and Monash Centre for Synchrotron Science, Monash University, Melbourne, Australia; and* [4]*Japan Synchrotron Radiation Research Institute, Hyogo, Japan*

Submitted 14 February 2011; accepted in final form 25 April 2011

Sonobe T, Schwenke DO, Pearson JT, Yoshimoto M, Fujii Y, Umetani K, Shirai M. Imaging of the closed-chest mouse pulmonary circulation using synchrotron radiation microangiography. *J Appl Physiol* 111: 75–80, 2011. First published April 28, 2011; doi:10.1152/japplphysiol.00205.2011.—Structural and functional changes of pulmonary circulation related to pathophysiology of pulmonary arterial hypertension (PAH) remain to be fully elucidated. Angiographic visualization in in vivo animals provided a powerful tool for assessing the major indexes associated with the pathogenesis of PAH. In this study, we have exploited the full potential of synchrotron radiation (SR) microangiography to show the ability to visualize pulmonary hemodynamics in a closed-chest mouse. Male adult mice were anesthetized and cannulated with a customized 24-gauge catheter into the right ventricle via the jugular vein for administering iodine contrast agent. The microangiography was performed on the left lung. We measured dynamic changes in vessel diameter in response to acetylcholine (ACh) and acute exposure to hypoxic gas (10% O_2). Moreover, the pulmonary transit time was estimated by the time of contrast agent circulating. We were able to visualize the pulmonary arteries from the left pulmonary artery (LPA) to the third generation of branching (inner diameter <100 μm). ACh and acute hypoxia induced vascular responses chiefly in the second and third branching vessels rather than the LPA and the first branching vessels. The transit time was only 0.83 s. These results demonstrate the effectiveness of SR for visualizing the pulmonary circulation in a closed-chest mouse. Future studies using SR microangiography on specific gene-targeted knockout and transgenic mice will provide new insights into the pathophysiology of pulmonary dysfunction and functional adaptation to survive in hypoxic condition.

angiography; pulmonary microvessels; pulmonary transit time

MANY OF THE UNDERLYING MECHANISMS responsible for the pathogenesis of pulmonary arterial hypertension (PAH) still remain to be fully elucidated. Functional changes in pulmonary microvessels are critical for modulating pulmonary blood flow, which is essential for optimizing ventilation-perfusion matching. Ultimately, dysfunction of the pulmonary microvasculature plays a pivotal role in the pathogenesis of several serious lung diseases. Visualization of the microvascular bed provides invaluable insight for evaluating vasoactive reactivity and, furthermore, understanding the underlying mechanisms that trigger early vessel disorders.

Address for reprint requests and other correspondence: M. Shirai, Dept. of Cardiac Physiology, National Cerebral and Cardiovascular Center Research Institute, 5-7-1 Fujishiro-dai, Suita, Osaka 565-8565, Japan (e-mail: shirai@ri.ncvc.go.jp).

In the last decade, the ability to produce targeted gene mutations in the mouse has provided a powerful tool for studying various pathophysiological pathways associated with PAH. One of the limiting factors for investigating pulmonary dynamics in a mouse model is its small size. Hence, the loss of spatial resolution restricts the use of more conventional angiography X-ray sources for assessing pulmonary blood flow distribution in small animals. Indeed, conventional X-ray angiography has resolution limitations for evaluating vessels with a diameter >200 μm (11, 13). Shirai et al. (20) designed a unique X-ray TV system for visualizing pulmonary vessels with diameters 100–500 μm, although the measurements were performed using open-chest animal models (21–23). However, in the last decade the technological advances of angiography using synchrotron radiation (SR) microangiography have provided the temporal and spatial resolution required to visualize microvessels of various organs both ex vivo and in vivo (12). Our previous report (17) demonstrated the visualization of lung vessels in the closed-chest rat and investigated functional changes of vessels in the setting of pulmonary hypertension (18, 19). Recently, a mouse model has been developed for imaging cerebrovascular vessels with diameters <150 μm (7).

The mouse model has become the preferred animal model for investigating the pathomechanisms that govern PAH, primarily because genetically engineered techniques more readily provide important new insights. Therefore, in this study, we have exploited the full potential of monochromatic SR microangiography to show, for the first time, the ability to visualize pulmonary hemodynamics in a mouse model in vivo.

MATERIALS AND METHODS

Animals. Experiments were conducted on eight male adult mice (C57BL/6, body weight: 25.9 ± 0.4 g). All mice were on a 12:12-h light-dark cycle at 24 ± 1°C and were provided with food and water ad libitum. All experiments were approved by the local Animal Ethic Committee of the National Cerebral and Cardiovascular Center Research Institute (Osaka, Japan) and conducted in accordance with the guidelines of the Physiological Society of Japan.

Surgical preparation. Mice were anesthetized by sodium pentobarbital (60 mg/kg ip). Supplementary doses of anesthetic were periodically administered (~15 $mg \cdot kg^{-1} \cdot h^{-1}$ ip). Throughout the experimental protocol, body temperature was maintained at 38°C using rectal thermistor coupled with a thermostatically controlled heating pad.

The trachea was cannulated, and the lungs were ventilated with a mouse ventilator (6 μl/g tidal volume and ~170–190 breath/min; Minivent Type 845; Harvard Apparatus). The inspirate gas was

enriched with oxygen, and the ventilator settings were previously shown to maintain arterial P_{CO_2} normocapnic condition.

A femoral vein was cannulated for acetylcholine (ACh) administration. A customized 24-gauge BD Angiocath catheter (Becton-Dickinson), with the tip bent at a 30° angle, was inserted into the jugular vein and advanced into the right ventricle for administering contrast agent as well as intermittently measuring right ventricular systolic pressure (RVSP) and heart rate (HR). RVSP signals were detected by BP transducer (MLT0670; ADInstruments), and signals were relayed to BP Amp (ML117; ADInstruments) and then continuously sampled at 1 kHz with a PowerLab system (ADInstruments) and recorded on a computer using Chart software (ADInstruments). HR was derived from the arterial systolic peaks. The mouse was securely restrained on the acrylic board in a supine position during surgical procedure. The plate was then fixed in a vertical position in front of the beamline so that the lung was positioned in front of SATICON X-ray detector.

Microangiographic system. The pulmonary imaging was performed with SR microangiography at the BL28B2 beam line of the SPring-8 facility (Hyogo, Japan). We have previously described in detail the accuracy and validity of SR for visualizing the pulmonary microcirculation in the closed-chest rat (17).

Briefly, monochromatic X-ray beam has a very narrow energy bandwidth for imaging (20–30 eV) at a flux ~1,010 photons·mm^{-2}·s^{-1}. This SR system comprised a monochromatic 33.2 keV X-ray source, just above the iodine K-edge energy for maximal contrast.

X-rays were detected by an X-ray detector (Hitachi Denshi Techno-Systems) incorporating a SATICON X-ray pickup tube (Hamamatsu Photonics) that was employed at the bending magnet beamline. The biomedical imaging SATICON X-ray camera has a resolution of 1,050 scanning lines and can record images at a maximum speed of 30 frames/s with shutter open times of 1.0~1.5 ms. High-resolution images were stored in a digital frame memory system with 1,024 × 1,024 pixel format and 10-bit resolution. Between recordings, the X-ray beam was blocked with Pb and Al filters.

Experimental protocol. The mouse was positioned in front of the beam line so that the left thorax was positioned in front of SATICON X-ray detector in alignment with the 9.5 × 9.5 mm imaging field. After verification of whether the imaging field comprised both the left lung vessels and heart, iodinated contrast agent (Iomeron 350; Bracco-Eisai) was injected via the jugular vein cannula. Angiography was performed with a microinjection pump (PHD-2000; Harvard Apparatus) that was programmed to deliver a bolus administration of 0.1 ml of iodine contrast agent at a speed of 10 ml/min. Image acquisition was initiated 1 s before iodine injection, and 100 frames were recorded for each scanning. The lung vessels were imaged when the ventilator was very briefly interrupted (<2 s) at end expiration to eliminate any movement artifact associated with the respiratory cycle. Mice were given at least 10 min to recover from each injection of contrast agent. The three-way stopcock on the right ventricle catheter was opened to collect RVSP after each imaging.

After baseline imaging was completed, mice were administered ACh (30 μg·kg^{-1}·min^{-1} iv) via the femoral vein cannula with continuous infusion pump (Pump 11; Harvard Apparatus). After 10 min, which was sufficient time for all cardiovascular variables to stabilize, lung microangiography was performed. During drug infusion, RVSP were continuously recorded, and then recording of RVSP was stopped and the stopcock was switched from the pressure transducer to the microinjection pump for imaging. After recovery from the ACh test, mice were exposed to acute hypoxia (10% O_2 balanced in N_2) for 5 min. The hypoxic gas mixture was prepared from N_2 and O_2 gas cylinders using gas mixer (GASCON; Kofloc). Lung microangiography was performed again after 5 min of acute hypoxic challenge.

Image analysis. Image analysis was performed as previously described (17), although slightly modified for mouse angiography. Vessels that belong to left lung were categorized according to branching level: left pulmonary artery (LPA; $n = 8$) and lobe artery branches (1st, $n = 15$; 2nd, $n = 26$; 3rd, $n = 12$~15 vessels). The computer-imaging program ImageJ (National Institutes of Health) was used to evaluate the vessel internal diameter (ID). To enhance images, a temporal subtraction operation was performed for flat-field correction using summation results of five consecutive frames acquired before contrast agent injection. The summation image taken before injection was subtracted from a single raw image taken after injection to eliminate the superimposed background structure. The ID of individual vessels was directly measured using Straight-Line-Selections tool of ImageJ. A 50-μm-thick tungsten wire, which had been placed directly across the corner of the detector's window, appeared in all of the recorded images and was subsequently used as a reference for calculating vessel diameter.

The pulmonary transit time of blood flow was estimated as contrast moved from the right ventricle to left ventricle using cine images of single scan at a speed of 30 frames/s. The number of frames was counted between the time contrast agent first appeared in the right ventricle to the time contrast appeared in the left ventricle. Subsequently, transit time was calculated.

Statistical analysis. All statistical analyses were conducted with GraphPad Prism 5 (GraphPad Software). All results are presented as means ± SE. One-way ANOVA was used to test for differences in baseline, ACh, and hypoxia in each parameter with the Bonferroni correction incorporated for multiple comparisons. A P value 0.05 was predetermined as the level of significance for all statistical analysis.

RESULTS

Baseline. The pulmonary circulation of the entire left lung could be clearly visualized in the anesthetized closed-chest mouse with iodinated agent. We observed, frame-by-frame, that contrast agent circulated from the right ventricle to left pulmonary vessels in real-time. Figure 1 shows a typical imaging pattern of left middle lung arteries from LPA to the second or third generation of branching with an ID <100 μm (Fig. 1, *top*). Vessel ID tended to decrease according to each generation of branching, as well as the distance away from the main axial artery toward the periphery. Generally in left lung images, LPA was 632.7 ± 24.4 μm. Thereafter, the first, second, and third branches were 274.3 ± 12.0, 154.0 ± 6.0, and 90.0 ± 2.2 μm, respectively (Fig. 1, *bottom*). The network of vessels from the LPA to the distal branches of the left lobe was observed in individual regions of interest (within the 9.5 × 9.5 mm imaging window).

Vasoactive response to ACh and acute hypoxia. Figure 2 presents the imaging of lung vascular responses to ACh (Fig. 2*B*) and acute hypoxia (Fig. 2*C*). Mice were administered ACh intravenously (30 μg·kg^{-1}·min^{-1}). ACh caused a small decline of RVSP but did not change in HR (Table 1). ACh induced significant dilation of the second and third branching vessels, evident by an increase in ID from 152.8 ± 7.0 to 173.4 ± 6.0 μm (2nd; Fig. 3) and from 90.0 ± 2.2 to 114.1 ± 4.4 μm (3rd; Fig. 3). The ID of the main LPA and first branch also tended to dilate, but there was no significance between baseline and ACh administration. One likely reason maybe due to the small number of vessels that were measured, and in particular, LPA was only in an image. Acute 10%-O_2 hypoxia induced significant vasoconstriction of the second and third order of branches (down to 108.6 ± 4.1 and 77.6 ± 2.6 μm, respectively; Fig. 3). Moreover, a considerable number of small vessels, <100 μm in diameter, were no longer visibly opaque following exposure to hypoxia, and the number of second or third branching vessels declined (Fig. 2). Despite the observa-

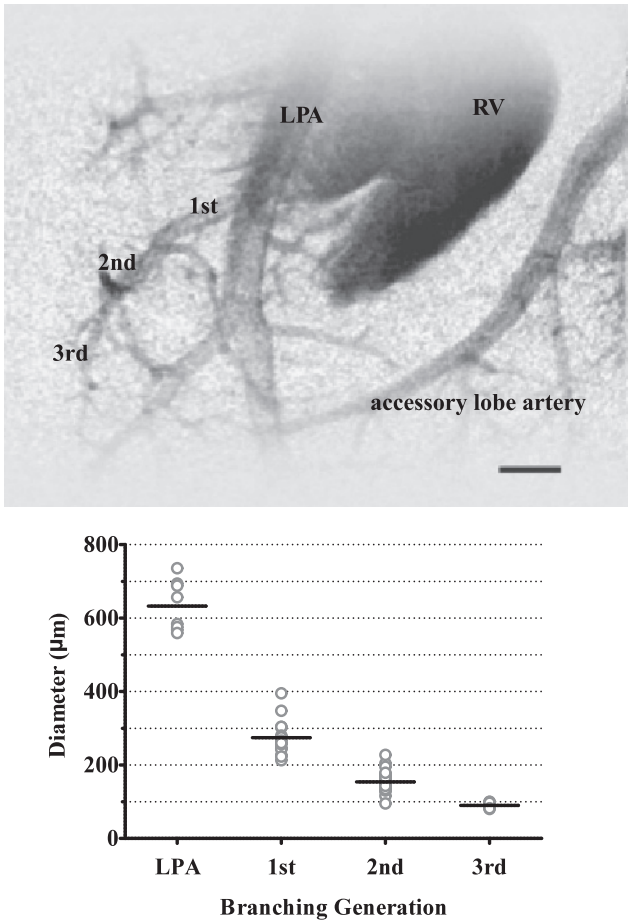

Fig. 1. *Top*: typical microangiogram image after temporal subtraction showing the branching pattern of small pulmonary arteries. Pulmonary branches to the second or third generation from the left pulmonary artery (LPA) were visible. Scale bar = 1,000 μm. *Bottom*: range of vessel size at each of the branching generations of pulmonary circulation in normal mice. RV, right ventricle.

tion that the first branching ID also tended to decrease, the diameter of LPA in the hypoxic lung appeared elevated (no significance), possibly because of the higher distending pressure for the hypoxic lung. During hypoxia, HR was decreased and RVSP was slightly increased due to the hypoxic vasoconstriction (Table 1).

Calculated pulmonary transit time. The cine images highlight the rapid clearance of contrast agent, enabling us to approximate the transit time of <1 s for blood circulating from right ventricle to left ventricle through the lung (Table. 1). Each single frame had a readout time of ~33 ms. Under baseline conditions, the small arterial branches were saturated with contrast agent within only ~7–10 frames from the time of injection The transit time from right ventricle to left ventricle was only 0.83 ± 0.03 s. ACh administration did not change the pulmonary transit time compared with baseline, but the time to saturation was positively extended in acute hypoxia. The delayed pulmonary transit time was 1.29 ± 0.15 s (Table. 1).

Table 1. *Hemodynamics data and estimated pulmonary transit time during experimental protocol*

	Baseline	ACh	Hypoxia 10% O_2
HR, beats/min	436 ± 31	431 ± 18	337 ± 23†
RVSP, mmHg	18.9 ± 0.8	16.7 ± 1.1	19.6 ± 1.9
Pulmonary transit time, s	0.83 ± 0.03	0.98 ± 0.03	1.29 ± 0.15*

Values are means ± SE (n = 6). HR, heart rate; RVSP, right ventricular systolic pressure; ACh, acetylcholine. *P < 0.05, †P < 0.01, significant differences from baseline.

DISCUSSION

The present investigation demonstrates the ability to clearly visualize pulmonary circulation in the lung of closed-chest anesthetized mouse using SR microangiography. We advanced the unique technique from our previous rat lung study and succeeded injecting the iodine contrast agent into the mouse right ventricle. Furthermore, we were also able to measure the changes in diameter of pulmonary vessels in response to ACh and the well-known pulmonary vasoconstrictor hypoxia, effectively demonstrating the reliability of using SR angiography for evaluating the pulmonary vascular responses.

SR microangiography. In the last decade, SR angiography has enabled visualization of small vessels that could not be seen using traditional conventional X-ray sources in closed-chest animals (17–19, 25). An earlier criticism of the temporal subtraction approach to using a single energy SR for angiography was that it was not suitable for in vivo imaging of dynamic organ systems, such as the heart and lungs, because organ motion causes vessel detection artifacts (5). However, as we and others (14, 17–19) have demonstrated recently, available detector systems permit rapid imaging and spatial resolution for accurate analysis of vessel caliber in the lungs and heart based on individual image frames.

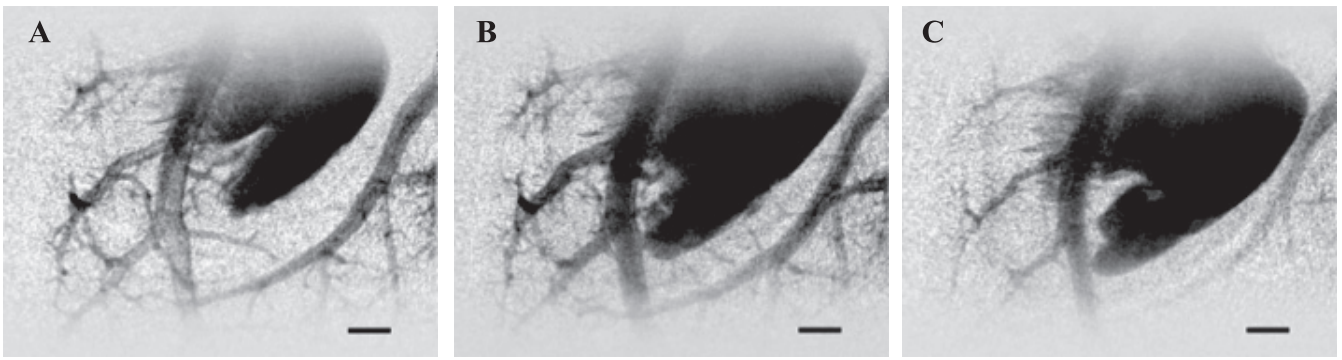

Fig. 2. Baseline microangiogram image (*A*) and typical images of response to acetylcholine (ACh) administration (*B*) and in response to acute 10% hypoxia (*C*). Smaller arteries partly disappeared in response to hypoxia (*C*). Scale bar = 1,000 μm.

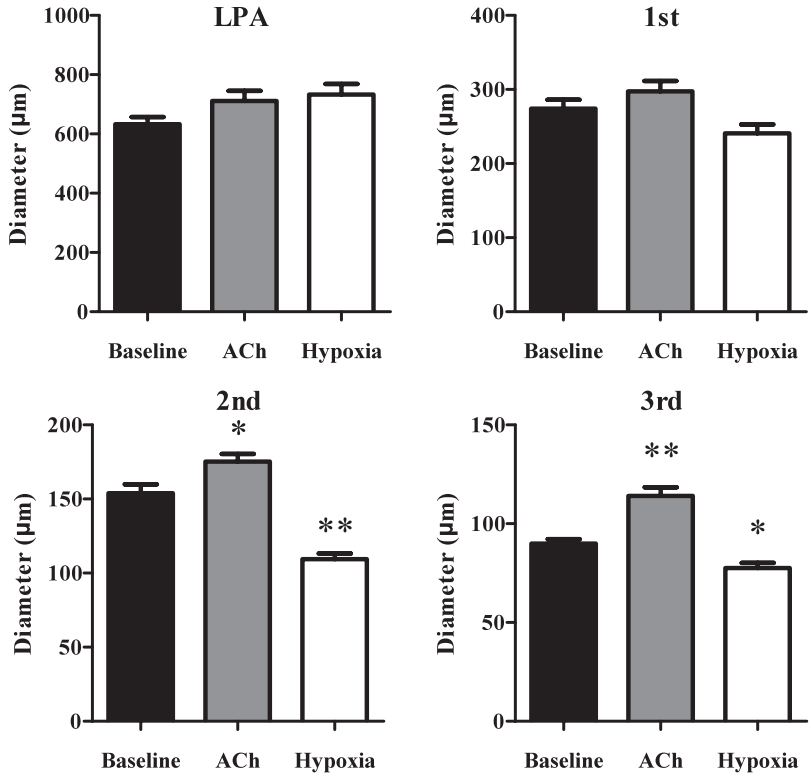

Fig. 3. Magnitude of response to ACh and acute hypoxic challenge in each measurable branching generation (LPA, n = 8; 1st, n = 15; 2nd, n = 26; 3rd, n = 12∼15 vessels). Data show means ± SE. *$P < 0.05$, **$P < 0.01$, significant difference from baseline.

In the SR imaging system, the smallest vessel detectable for measuring ID is primarily determined by the concentration of iodine contrast agent. The iodine concentration depends on the dose of the contrast agent, the injection technique, and the dilution curve and the vessel site of interest. In the present study, contrast agent was injected into the right ventricle so that the iodine concentration within the pulmonary circulation would have been diluted by venous return. However, the rate at which contrast agent was injected (10 ml/min) is approximately equivalent to cardiac output of anesthetized mouse (∼10 ml/min; Refs. 2, 6). Therefore, even if the bolus dose were diluted, a preliminary phantom study (18) has previously shown that vessel edge detection should be accurate and reproducible for vessels with an ID as small as 100 μm. One limitation, however, is that a large bolus of contrast agent is required for each injection due to the high speed of clearance depending on HR. Although we could not measure the hemodynamics during each bolus injection, blood pressure and HR were intermittently monitored after injecting and image capturing were completed. Then, we confirmed the hemodynamics were stable and had recovered to preinjection values.

Change of pulmonary vasculature. In our previous study, the diameters of the pulmonary arteries were reported in rats, as measured by SR microangiography (17). That study clearly highlighted the diverse vessel branching pattern from the first to fourth generation of branching (ID <100 μm). The advantage of using a closed-chest mouse model in the present study was that we could visualize, not only LPA and first to third branching generations, but also numerous precapillary arterioles (ID <80 μm) in a single frame of imaging (Fig. 1). The vascular responses to ACh and hypoxia were measurable even in the arteriole level, which showed significant responses (Fig. 3). A single frame covered an area one third of the left lung (Sonobe T, et al., unpublished observations), suggesting the size of the mouse lung is better suited for evaluating global changes of the pulmonary vascular tree including resistance vessels and nonresistance vessels simultaneously. Although smaller vessels exist within the pulmonary vascular bed of both the mouse and rat, we were unable to clearly detect the border of these vessels. This suggests that the resolution limit of the pulmonary microvessels in this imaging system was close to 80 μm. Spatial resolution was limited in pulmonary vessels in vivo, because of the possibility of nonuniform constrictions or uneven iodine contrast distribution within the smaller vessels, which would increase the signal-to-noise variability between neighboring pixels of any single image. Considering the morphology, casting models often provide powerful evidence for understanding the pulmonary vascular system (24). Although semiquantification may be possible by casting, detecting rapid physiological change of vessel diameter (e.g., response to ACh or hypoxia) can be performed accurately only by angiography.

Measurement of pulmonary transit time. A further significant advantage of using mice for SR pulmonary angiography is that the field of view (nearly 1 cm^2) covers both left lung and heart in a single image. Moreover, since the image recording system permits recording of 30 frames/s, it is possible to trace the flow of contrast agent in vessels. Therefore, this system has the potential to measure, not only ID, but also transit time in the pulmonary vascular bed. The cine images highlight the rapid clearance of contrast agent, enabling us to approximate the transit time within a second for blood to circulate through the left lung (Table 1). Actually, we counted the frame number during contrast agent circulating through left lung from right ventricle to left ventricle.

Pulmonary transit time is determined by many cardiopulmonary factors (e.g., cardiac output, systemic and pulmonary

vascular resistance, and HR); therefore, transit time provides invaluable information concerning cardiopulmonary status in cardiac or lung disease. Some previous reports have evaluated pulmonary capillary transit time using isolated or excised lung of various animals (1, 3, 10, 15). Sada et al. (16) performed the measurement of pulmonary transit time using anesthetized cat lung; however, the pulmonary transit times have been not measured at real-time resolution in living mouse. Lindstedt (9) has shown the predicted capillary transit time of mammalian lung. Specifically, the capillary transit time of the white mouse (body wt: 42 g) was estimated to be 0.59 s at rest. In our study, we observed that the pulmonary transit time for mice, with a body weight of ~30 g, was 0.83 s at rest. We did not measure "capillary" transit time because of overlapping of contrast agent in the arteries and veins. The injected contrast agent quickly passed through gas-exchanging vessels depending on the high HR (>400), and then, arteries, capillaries, and veins were all depicted in a single frame. Nonetheless, the mouse pulmonary transit time that we measured is comparable to that of previous studies. Kreissl et al. (8) demonstrated the transit of radiotracer from right ventricle to left ventricle in mouse using high-temporal-resolution small animal PET, and the data indicated that the transit time is within one second. Furthermore in this study, when mice were exposed to acute hypoxic challenge, the transit time was significantly prolonged to 1.29 s (Table 1) vs. resting transit time. The architecture of the vascular network is a major determinant of the distribution of transit time in the organs. Pulmonary hypoxic vasoconstriction was evident in the present study, which was reflected by a small increase in RVSP, although there are distinct decreases of HR (Table 1). Clough et al. (4) reported the dog pulmonary transit time in hypoxic conditions using an isolated lung model. They demonstrated a stable pulmonary flow under normoxic conditions, and, moreover, transit time was significantly shortened during hypoxia (4). Since a potential decrease in cardiac output and HR would reduce blood flow, it could be expected that transit time increased in our intact lung study. We also noted that ACh administration tended to prolong the transit time, which may presumably be linked to a decrease in cardiac output.

PAH study using mouse model. Many respiratory disorders, such as pulmonary hypertension, are characterized by abnormal structural and functional changes in the pulmonary microcirculation. Our prior work (18, 19) demonstrated the distribution of pulmonary blood vessels using SR microangiography in a closed-chest rat model with PAH. The SR microangiography was effective for visualizing dynamic and regional changes in vessel caliber; however, the rat model focused on a narrow region of the pulmonary circulation. In the present study, we established the mouse model that enabled visualizing both lung and heart in the closed chest. Therefore, the mouse model has a potential to provide important insight into the lung vascular physiology, for example, differences in regional control of pulmonary blood flow throughout the whole lung or the complex interaction between pulmonary and cardiac regulation of blood flow. One of the most important advantages of pulmonary imaging in mice is the potential to use genetic "knockout" models in future studies. They will provide new insights into the pathophysiology of pulmonary dysfunctions and functional adaptation. Using these techniques, we are planning to investigate the functional changes of pulmonary vessels under hypoxic conditions with various knockout mice.

Summary. The use of SR microangiography provides a powerful tool for assessing pulmonary hemodynamics in unprecedented detail in a mouse model. Importantly, this now provides us with the ability to assess the various neurohumoral pathways that modulate the pulmonary vasculature in specific gene-targeted knockout and transgenic mice. Ultimately, future studies using SR microangiography on transgenic mice will provide important new insights into the pathophysiology of pulmonary dysfunctions and functional adaptation.

ACKNOWLEDGMENTS

We are extremely grateful for the use of the SPring-8 facilities. The SR experiments were performed at the BL28B2 at SPring-8 with the approval of the Japan Synchrotron Radiation Research Institute.

GRANTS

This work was supported in part by a Research Grant for Cardiovascular Disease (21A-13) from the Ministry of Health, Labour, and Welfare of Japan and a Grant-in-Aid for Scientific Research (20590242) from the Ministry of Education, Culture, Sports, Science, and Technology of Japan.

DISCLOSURES

No conflicts of interest, financial or otherwise, are declared by the author(s).

REFERENCES

1. **Ayappa I, Brown LV, Wang PM, Katzman N, Houtz P, Bruce EN, Lai-Fook SJ.** Effect of blood flow on capillary transit time and oxygenation in excised rabbit lung. *Respir Physiol* 105: 203–216,1996.
2. **Champion HC, Villnave DJ, Tower A, Kadowitz PJ, Hyman AL.** A novel right-heart catheterization technique for in vivo measurement of vascular responses in lungs of intact mice. *Am J Physiol Heart Circ Physiol* 278: H8–H15, 2000.
3. **Clough AV, Haworth ST, Hanger CC, Wang J, Roerig DL, Linehan JH, Dawson CA.** Transit time dispersion in the pulmonary arterial tree. *J Appl Physiol* 85: 565–574, 1998.
4. **Clough AV, Haworth ST, Ma W, Dawson CA.** Effects of hypoxia on pulmonary microvascular volume. *Am J Physiol Heart Circ Physiol* 279: H1274–H1282, 2000.
5. **Dill T, Dix WR, Hamm CW, Jung M, Kupper W, Lohmann M, Reime B, Ventura R.** Intravenous coronary angiography with synchrotron radiation. *Eur J Phys* 19: 499, 1998.
6. **Janssen BJ, De Celle T, Debets JJ, Brouns AE, Callahan MF, Smith TL.** Effects of anesthetics on systemic hemodynamics in mice. *Am J Physiol Heart Circ Physiol* 287: H1618–H1624, 2004.
7. **Kidoguchi K, Tamaki M, Mizobe T, Koyama J, Kondoh T, Kohmura E, Sakurai T, Yokono K, Umetani K.** In vivo X-ray angiography in the mouse brain using synchrotron radiation. *Stroke* 37: 1856–1861, 2006.
8. **Kreissl MC, Wu HM, Stout DB, Ladno W, Schindler TH, Zhang X, Prior JO, Prins ML, Chatziioannou AF, Huang SC, Schelbert HR.** Noninvasive measurement of cardiovascular function in mice with high-temporal-resolution small-animal PET. *J Nucl Med* 47: 974–980, 2006.
9. **Lindstedt SL.** Pulmonary transit time and diffusing capacity in mammals. *Am J Physiol Regul Integr Comp Physiol* 246: R384–R388, 1984.
10. **Maseri A, Caldini P, Permutt S, Zierler KL.** Frequency function of transit times through dog pulmonary circulation. *Circ Res* 26: 527–543, 1970.
11. **McDonald DM, Choyke PL.** Imaging of angiogenesis: from microscope to clinic. *Nat Med* 9: 713–725, 2003.
12. **Mori H, Hyodo K, Tanaka E, Uddin-Mohammed M, Yamakawa A, Shinozaki Y, Nakazawa H, Tanaka Y, Sekka T, Iwata Y, Handa S, Umetani K, Ueki H, Yokoyama T, Tanioka K, Kubota M, Hosaka H, Ishikawa N, Ando M.** Small-vessel radiography in situ with monochromatic synchrotron radiation. *Radiology* 201: 173–177, 1996.
13. **Myojin K, Taguchi A, Umetani K, Fukushima K, Nishiura N, Matsuyama T, Kimura H, Stern DM, Imai Y, Mori H.** Visualization of

intracerebral arteries by synchrotron radiation microangiography. *Am J Neuroradiol* 28: 953–957, 2007.
14. **Pearson JT, Schwenke DO, Jenkins MJ, Edgley AJ, Sonobe T, Ishibashi-Ueda H, Umetani K, Eppel GA, Evans RG, Okura Y, Shirai M.** Benefits of synchrotron microangiography for dynamic studies of smooth muscle and endothelial roles in the pathophysiology of vascular disease. *AIP Conf Proc* 1266: 84–88, 2010.
15. **Presson RG Jr, Todoran TM, De Witt BJ, McMurtry IF, Wagner WW Jr.** Capillary recruitment and transit time in the rat lung. *J Appl Physiol* 83: 543–549, 1997.
16. **Sada K, Shirai M, Ninomiya I.** X-ray TV system for measuring microcirculation in small pulmonary vessels. *J Appl Physiol* 59: 1013–1018, 1985.
17. **Schwenke DO, Pearson JT, Umetani K, Kangawa K, Shirai M.** Imaging of the pulmonary circulation in the closed-chest rat using synchrotron radiation microangiography. *J Appl Physiol* 102: 787–793, 2007.
18. **Schwenke DO, Pearson JT, Kangawa K, Umetani K, Shirai M.** Changes in macrovessel pulmonary blood flow distribution following chronic hypoxia: assessed using synchrotron radiation microangiography. *J Appl Physiol* 104: 88–96, 2008.
19. **Schwenke DO, Pearson JT, Shimochi A, Kangawa K, Tsuchimochi H, Umetani K, Shirai M, Cragg PA.** Changes in pulmonary blood flow distribution in monocrotaline compared with hypoxia-induced models of pulmonary hypertension: assessed using synchrotron radiation. *J Hypertens* 27: 1410–1419, 2009.
20. **Shirai M, Sada K, Ninomiya I.** Effects of regional alveolar hypoxia and hypercapnia on small pulmonary vessels in cats. *J Appl Physiol* 61: 440–448, 1986.
21. **Shirai M, Shindo T, Ninomiya I.** β-Adrenergic mechanisms attenuated hypoxic pulmonary vasoconstriction during systemic hypoxia in cats. *Am J Physiol Heart Circ Physiol* 266: H1777–H1785, 1994.
22. **Shirai M, Shindo T, Shimouchi A, Ninomiya I.** Diameter and flow velocity changes of feline small pulmonary vessels in response to sympathetic nerve stimulation. *Pflügers Arch* 429: 267–273, 1994.
23. **Shirai M, Pearson JT, Shimouchi A, Nagaya N, Tsuchimochi H, Ninomiya I, Mori H.** Changes in functional and histological distributions of nitric oxide synthase caused by chronic hypoxia in rat small pulmonary arteries. *Br J Pharmacol* 139: 899–910, 2003.
24. **Sun XZ, Inouye M, Takahashi S, Fukui Y.** Pulmonary vascular system in young mice using corrosive resin cast technique. *Environ Med* 42: 167–169, 1998.
25. **Tokiya R, Umetani K, Imai S, Yamashita T, Hiratsuka J, Imajo Y.** Observation of microvasculatures in athymic nude rat transplanted tumor using synchrotron radiation microangiography system. *Acad Radiol* 11: 1039–1046, 2004.